


# Geometry optimization in buckling of a shape memory alloy column due to constrained recovery

Journal of Intelligent Material Systems and Structures  
23(1) 65–76  
© The Author(s) 2011  
Reprints and permissions:  
sagepub.co.uk/journalsPermissions.nav  
DOI: 10.1177/1045389X11430730  
jim.sagepub.com  


Kunavar Janez, Kosel Franc, Pukšič Andrej and Videnič Tomaž

## Abstract

Constrained recovery of a compressively prestrained shape memory alloy (SMA) is experimentally and theoretically investigated. Thermomechanical properties of the SMA during the process of constrained recovery are experimentally obtained. Optimization of geometry in buckling of an ideally straight, simply supported column with a nonconstant cross section due to constrained recovery is theoretically investigated. Using the experimentally obtained thermomechanical properties, the critical buckling force and temperature of the optimized column are calculated. Various experiments were conducted in order to verify the calculated results. The calculated critical load and predicted buckling temperatures show good agreement with buckling experiments reported in this article.

## Keywords

shape memory alloy, constrained recovery, optimization of geometry in buckling of columns

## Introduction

Intelligent material is, etymologically speaking, every material that inherits some hidden information, while the engineer is trying to uncover and understand as much of this information and use it for his innovative design. An important branch of materials that is extensively investigated is shape memory alloy (SMA). The shape memory effect is a unique property of some alloys, which, after being deformed at lower temperature, recover their original shape when heated to a higher temperature. The so-called memory is a result of the reversible martensitic transformation, which is a solid–solid, diffusionless transition between a crystallographically less ordered, low-temperature product phase (martensite) and a crystallographically more ordered, high-temperature parent phase (austenite). The return to the original shape starts at the austenite start temperature  $A_s$  and completes at the austenite finish temperature  $A_f$  (Brinson, 1993). On the other hand, if the SMA is cooled from the austenitic phase, it starts to transform back to martensite at a temperature called martensite start temperature  $M_s$  and ends at the martensite finish temperature  $M_f$  (Brinson, 1993). In this way, large strains of up to 8% (Duerig et al., 1990) can be recovered during heating from martensite to austenite, and the process is often referred to as reverse martensitic transformation or free recovery. If free recovery is hampered by an external obstacle before temperature,

$A_f$  is reached, large recovery stresses up to 800 MPa (Duerig et al., 1990) can be generated during heating, and the process is called constrained recovery (Šittner et al., 2000; Stalmans et al., 1997). This property makes SMAs ideally suited for use as fasteners, clamps, and medical elements since it ensures constant load at various changes of strain during usage (Duerig et al., 1990, 1999). Of particular importance for such applications is an understanding of the generation of recovery stresses with respect to temperature (Kosel and Videnič, 2007; Videnič et al., 2008). Another property of SMA is the so-called pseudoelastic effect, where austenite in the SMA during loading can transform to martensite. This transformation is performed at constant load and considerable strain, where during unloading, SMA transforms to austenite and returns to original shape.

Buckling of columns is a stability problem, extensively researched for many years (Bažant and Cedolin, 1991; Shanley, 1957; Timoshenko, 1961). However, buckling of structural elements produced from SMAs is a relatively new topic. Among the authors who have

---

Faculty of Mechanical Engineering, University of Ljubljana, Ljubljana, Slovenia

## Corresponding author:

Kunavar Janez, Faculty of Mechanical Engineering, University of Ljubljana, Aškerčeva 6, 1000 Ljubljana, Slovenia  
Email: kujanez@gmail.com

dealt with this problem, we can mention Lee and Jung (1999), who numerically solved buckling of a composite shell reinforced with SMA wires, where SMA contraction under shape memory effect causes a compressive force to its composite surrounding. Rahman et al. (2001, 2005) experimentally and numerically researched buckling of a SMA column where buckling appears due to the effect of superelasticity, which is another property of SMAs. Movchan and Sil'chenko (2003) report an analytical and experimental study of the buckling of SMA columns during transformation from austenite to martensite.

The mechanism of buckling due to thermal expansion is used for activation in more complex temperature switch systems in electromechanical devices. Motivated by the possibility of this kind of application, we here explore the process of constrained recovery of a SMA column, which could perform such a task. To our knowledge, research on buckling of SMA columns due to constrained recovery has not been reported so far in the available literature.

In the present article, a particular case of constrained recovery is observed, such that the generated stress is compressive. At a certain temperature, the generated compressive stress can induce loss of the column's stability if the column is too slender. Research was conducted to understand the process of buckling due to constrained recovery for a column with nonconstant cross section. The experimental part of the research consists of measuring the thermomechanical properties, followed by experiments of constrained recovery. The theoretical part consists of obtaining equations for elastic modulus and compressive force as functions of temperature during constrained recovery. Buckling of columns in the elastic domain is used to obtain the optimal shape of the SMA column and to calculate the buckling force and temperature for various shapes of an ideally straight SMA column. A set of experiments was made to verify the correctness of the calculated buckling forces and temperatures.

## Problem Definition

To achieve a process of constrained recovery, prestrain must be applied to a specimen, which can be performed by different methods (Sittner et al., 2000). Compression prestrain of a 100% martensite phase was chosen in our case as the most practical, also in view of potential use. After the prestrain is applied, the specimen (ideally a straight SMA column with circular cross section) is put between simple supports, with zero axial travel. During heating up to  $A_s$ , compressive stress appears due to thermal expansion of the SMA specimen. Heating to temperatures above  $A_s$  triggers the process of constrained recovery, which causes additional compressive stress. The observed specimen is supposed to buckle at

some temperature in the temperature range between  $A_s$  and  $A_f$ , where compressive stress is rising with the highest rate during heating. Our goal is to obtain the optimal shape of the column with circular cross section, such that it will have maximum buckling force at the same volume and length compared with nonoptimized shape.

In order to calculate the buckling force  $F_b$ , we must first determine the compressive force and mechanical properties (both as function of temperature during process of constrained recovery of SMA column). The recovery force for columns with nonconstant cross section can be calculated, using physical models where constrained recovery is solved (Kato et al., 2004; Kosel and Videnič, 2007) or obtained experimentally. The mechanical property that is observed before resolving the buckling problem is the stress–strain diagram at buckling temperature. Linear elastic, nonlinear elastic, and elastoplastic type of stress–strain diagram could be possible. However, there is no particular information in the literature as to what type of diagram should be used; therefore, without employing adequate experiments, this diagram cannot be precisely predicted (Kato et al., 2004; Movchan and Sil'chenko, 2003; Stalmans et al., 1997).

If it turns out that the stress–strain diagram at buckling temperature shows an elastic relation, it is enough to know the compressive stress and elastic modulus of the phase mixture at buckling temperature to describe both the external load and stress–strain diagram of the specimen at buckling temperature.

It is a well-known fact that the elastic modulus of the austenite phase  $E_a$  is higher (in the range of 2–3 times) than the elastic modulus of the martensite phase  $E_m$ , depending on type of SMA (Brinson, 1993). During heating above  $A_s$ , the reverse martensitic transformation is in progress and the volume fraction of martensite is diminishing. The volume fraction of martensite is denoted by  $\xi$  and defined as  $\xi = V_m / (V_a + V_m)$ , where  $V_m$  is the volume of martensitic and  $V_a$  the volume of austenitic phase present in the SMA column (Brinson, 1993). Since, during the transformation progress, both phases coexist ( $\xi$  is between 1 and 0), the elastic modulus of the phase mixture  $E$  is neither  $E_a$  nor  $E_m$ . It can be assumed that  $E$  is a function of  $\xi$ . The volume fraction  $\xi$  is a function of temperature, as well as a function of the applied stress on the column. However, during the process of constrained recovery, the applied stress is also a function of temperature. Therefore, the relation  $\xi(T)$  should be obtained in order to determine the dependence of the elastic modulus of the phase mixture on temperature. There are models available in the literature where  $\xi(T)$  and recovery stress  $\sigma(T)$  can be calculated during the process of constrained recovery (Kosel and Videnič, 2007; Videnič et al., 2008).

Obtaining  $\xi(T)$  is sufficient only for the case of linear elastic type of the stress–strain diagram at buckling

temperature; therefore, an experimental way to define the stress–strain diagram at predicted buckling temperature is proposed. The experimental results will also show the type of aforementioned stress–strain relation of the specimen at different temperatures.

For better understanding, consider that compressive tests with a loading up to 0.5% of compressive strain followed by an unloading at constant temperature  $T > A_s$ , are to be made in order to get the stress–strain diagram. Such tests are to be made at different temperatures in order to get stress–strain diagrams at different possible buckling temperatures. The most important information is if the specimen is hampered during heating from room temperature  $T_0$  to  $T$ . Usual method for obtaining stress–strain diagram is normally understood as a compressive test at constant temperature  $T > A_s$ , where the SMA specimen is not hampered while heating to  $T$ . While heating the specimen to the testing temperature, the process of reverse martensitic transformation occurs, and at the start of test at  $T > A_s$ , the specimen has some phase mixture, described by  $\xi_1$ . However, in this article a different method was used, which more precisely resembles the problem of buckling due to constrained recovery. By this method, the specimen is prestrained when it is in the martensitic phase at a temperature lower than  $M_f$  and then hampered while heating to temperature  $T > A_s$ . The process of constrained reverse martensite transformation occurs with a resulting phase mixture  $\xi_2$  at the start of the compressive test, when it is different from  $\xi_1$ .

## Experimental Setup

Experiments were designed in order to obtain two main sets of results. The first set of experiments was made to obtain thermomechanical characteristics of SMA specimens during the process of constrained recovery, and the second set of experiments was made to obtain the critical buckling temperature of SMA specimens. A brief description of each component of the testing apparatus is given in the following.

### Loading and Measuring System

Tests were conducted on a Zwick Z050/TH3A testing machine, with a maximum tensile/compression force of 50 kN, within a precision range of  $\pm 0.5$  N. The force was supplied by an electrically driven spindle placed in the frame of the testing machine and measured by a strain gauge measuring cell.

The strain of the specimen was measured by an extensometer travel measuring. Zwick extensometers suited to maximum measurement temperature of 250°C with precision range within  $\pm 0.2$   $\mu\text{m}$  were used.

The control unit of the testing machine was interfaced with an Intel PC/Pentium computer, with

TextXpert II software used for collecting and storing data and data analysis.

### Heating and Cooling System

Tests were carried out in a ventilated temperature chamber, produced by Zwick. The temperature range of the chamber is between  $-70^\circ\text{C}$  and  $250^\circ\text{C}$ , with ability to keep constant preset temperature in the range of  $\pm 0.1^\circ\text{C}$ . Heating of air was provided by an electric heater and air ventilating system to ensure homogenous air temperature in the temperature chamber. The temperature chamber was controlled *via* TestXpert II software.

Factory-fitted thermometers in the temperature chamber measure air temperature in the temperature chamber. Some experiments require the temperature of the specimen to be measured more accurately. In such cases, the temperature of air may not be the same as the temperature of the specimen; therefore, an extra K-type thermocouple was used to measure the specimen temperature.

### Specimen Properties

The specimens used for tests were produced from Ni–Ti 50% alloy. The manufacturer, Memry<sup>®</sup> GmbH, estimated the transformation temperature  $A_f = 65^\circ\text{C}$ . The exact details on thermomechanical history of the obtained SMA material are not given. Therefore, transformation temperatures were obtained by standard experimental method (Duerig et al., 1990) with thermal cycle (heating from  $20^\circ\text{C}$  to  $100^\circ\text{C}$  and cooling down to  $20^\circ\text{C}$  at a rate of  $1^\circ\text{C}/\text{min}$ ) of the specimen under constant uniaxial tensile stress, while measuring displacement of the specimen. After one thermal cycle, transformation temperatures were obtained from the diagram of temperature–displacement. Experiments were conducted on three different levels of tensile stress, in order to obtain the diagram of transformation temperatures–tensile stress. From this diagram, it is observed that  $M_f = 27^\circ\text{C}$ ,  $M_s = 30.5^\circ\text{C}$ ,  $A_s = 57^\circ\text{C}$ , and  $A_f = 67^\circ\text{C}$ . Stability of shape memory effect is assured by the manufacturer, and it is also presented *via* experiments (Figure 3). The specimens had the shape of straight bars of circular cross section with a diameter of 3.12 mm and length of 200 mm. For later tests, different lengths of specimens were prepared.

## Experimental Determination of Thermomechanical Properties during Constrained Recovery

### Test Procedure

Specimens for experiments in this article were cut to a length of 40 mm. Testing procedure consists of four main stages: in the first stage, the specimen is prepared



to reset any previous deformations and to reach a 100% martensitic phase. This stage consists of heating the specimen on an electric heating plate to 150°C for 2 min, slowly cooling it down and leaving it in a freezer at  $-8^{\circ}\text{C}$  for 5 min.

In the second stage, compressive prestrain of the specimen in the martensitic phase is applied. Transformation temperatures obtained in the experiments indicate that the room temperature (around 25°C) is under  $M_f$ . Therefore, martensite prestrain can be obtained at room temperature. To achieve this, the specimen is put between the clamping jaws of the testing machine, into a specially designed gripping device, as shown in Figure 1. The gripping device prevents possible buckling of the specimen under compressive stress, and after the specimen is put inside this device, there is an axial distance  $\Delta_a$  of approximately 3 mm between the facing planes of the gripping device. The diameter of the borehole in the gripping device, where the specimen is fit, ensures a loose tolerance between the borehole and specimen. At room temperature, the specimen is compressed at a clamping jaw rate of 0.5 mm/min, until compressive strain reaches 2.5%, and then the specimen is unloaded to zero stress. After unloading, there is approximately 2% of compressive strain present in the specimen, and this is called prestrain  $\epsilon_{s,0}$ .

In the third stage, the specimen remains in the gripping device, and the software keeps the distance between the extensometer constant during the following test. The extensometers are put on the specimen body between clamping jaws. Then the air temperature in the temperature chamber starts to rise at a rate of 1°C/min, and it keeps rising until it reaches the preset target temperature, higher than  $A_s$ , where it is kept constant for 1 min. During this heating process, there is an increase in the compressive stress in the specimen, that is, below  $A_s$  due to thermal expansion, while at temperatures above  $A_s$  additional stress appears because of constrained recovery.

The fourth stage starts by keeping the air temperature in the chamber at constant target temperature for 1 min. Additional compressive strain is applied to the specimen

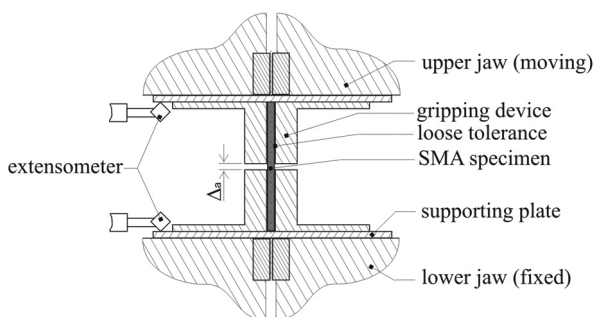


**Figure 1.** Specimen fits between upper and lower jaw of testing machine.

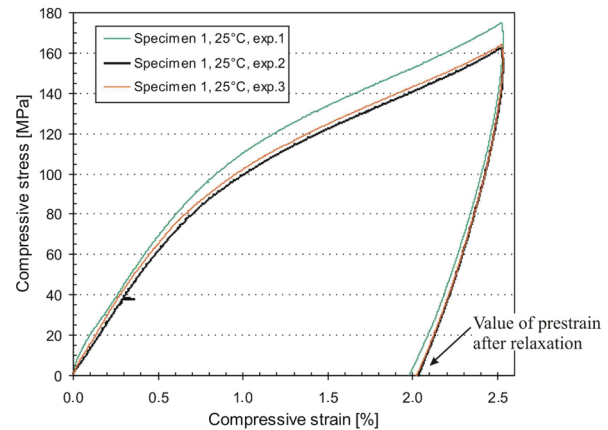


**Figure 2.** Obtaining compressive prestrain at room temperature.

by moving the jaws together at a rate of 0.5 mm/min, and then the jaws are moved apart until compressive stress is zeroed. During all the phases of this test, the temperature of the specimen is measured with a K-type thermocouple placed inside the gripping device.

## Results

As described earlier in section ‘Test Procedure’, experiments are conducted on the same specimen, until the target temperature is reached and additional stress applied. Six target temperatures were examined: 60°C, 68°C, 72°C, 77°C, 80°C, and 90°C, respectively. Figure 2 presents the second stage of the experiment, namely compressive prestrain and unloading until an approximate 2% compressive strain is reached at a room temperature of 25°C. Three different results of this stage of experiment are presented in Figure 2, where a good agreement between each value of prestrain after deformation is observed.

The third stage of the experiment described in section ‘Test Procedure’ is constrained recovery of the specimen. A graph of compression stress versus temperature of this experimental stage is shown in Figure 3 for three experiments of the same specimen. From Figure 3, some oscillation in compressive stress during heating can be noticed. This problem is present at all tests, where the testing machine during heating had to ensure constant zero strain, measured *via* extensometers. Such control cycle is particularly demanding during reverse martensite transformation, where the testing machine must keep zero strain at a higher stress rate due to constrained recovery. In Figure 3, additional compressive strain in the first experiment (green line) is 0.15%, while the next two experiments are made with 0.3% additional compressive strain.

The fourth stage of experiment consists of additional compressive strain at constant target temperature, as shown in compressive stress–strain diagram.

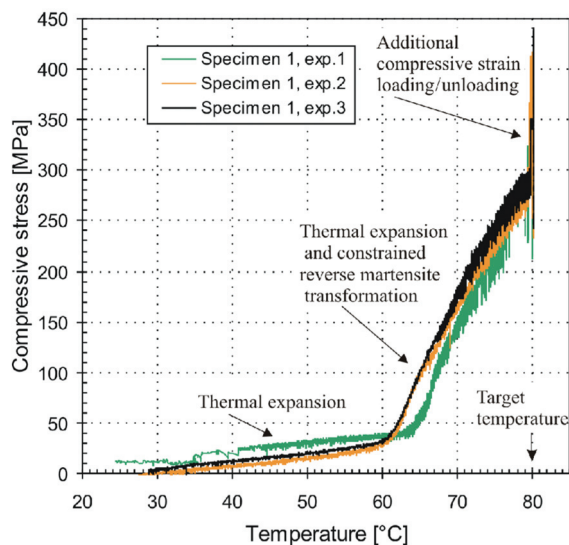


**Figure 3.** Compression stress versus temperature at constrained recovery.

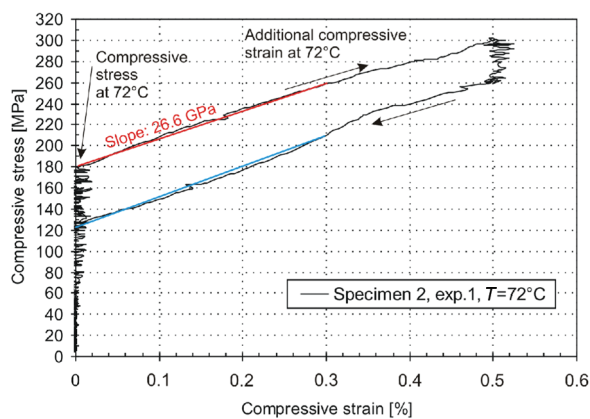


**Figure 4.** Additional compressive stress–compressive strain.

In Figure 4, this stage is presented for the target temperature of 72°C, with the main part of martensite in the phase mixture, as can be seen by the value of slope. It is shown that after additional compressive strain is applied, there is a linear relationship between additional compressive stress and compressive strain. Therefore, it can be assumed that the slope of the aforementioned linear relationship in Figure 4 is the elastic modulus of phase mixture in the specimen at different target temperatures. During unloading, the stress–strain relation can also be linearized (Figure 4, lower line), where its slope, that is, elastic modulus, is the same in the case of loading and unloading. Some difference in the path between loading and unloading is noticed, but it can be explained as a problem of the testing machine in keeping a constant rate of strain, particularly at the start of unloading. Therefore, this difference will be neglected, and the path at loading will be considered the same as

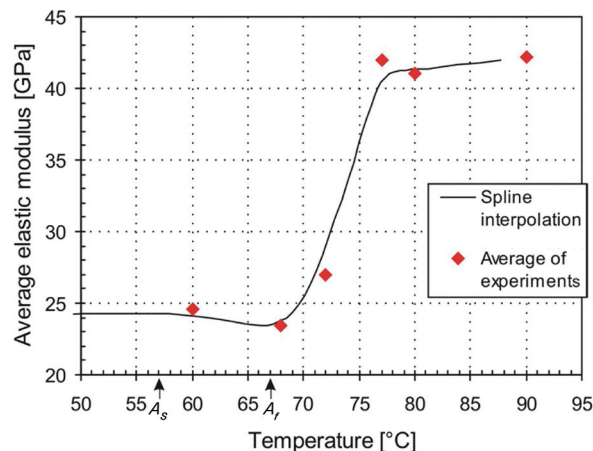


**Figure 5.** Average elastic modulus at target temperatures.

the path of unloading in the stress–strain diagram. By doing so, the SMA specimen is now supposed to behave as an elastic material, but it must be taken into account that the elastic modulus of this material is a function of temperature,  $E(T)$  (for a column with constant cross section). This function is obtained by experiments and presented in Figure 5.

At each target temperature, three experiments were performed in order to obtain an average value of compressive stress due to constrained recovery and to obtain the average value of elastic modulus. Between average experimental results, spline interpolation is constructed using Mathematica software. The rate of change in the elastic modulus is the highest in the range between 67°C and 77°C, as shown in Figure 5. This is the temperature range with the most intense reverse martensitic transformation. High compressive stress can appear during additional compression, especially at temperatures above 72°C; therefore, the possibility of the martensite transformation must be explained. Martensite transformation starts at the line, with origin at  $M_s$  (Figure 5), where the slope of this line was obtained from experiments as  $\tan\beta = 10.5 \text{ MPa/K}$ . Therefore, theoretical martensite transformation stress at 80°C is 520 MPa, which is higher than measured values that are in the range of 440 MPa, meaning that transformation theoretically cannot occur. Also, martensite transformation due to additional compression was not observed in our experiments.

### A Simple One-Dimensional Model of Constrained Recovery in Shape Memory Alloys with Nonconstant Cross Section

Preparation and thermomechanical procedure to achieve buckling of the specimen were presented earlier in this article. The aim of geometry optimization is to achieve such geometry of the column that would

withstand maximum load capacity at its minimum mass. One of the design criteria of slender structural members is to consider a possible nonstable stage at maximum load. This can be accomplished by rearranging the material so that a maximal cross section is prescribed for the structural member in regions with higher stress.

In our case, the buckling of columns with circular cross section is dealt with where the optimization criterion is for a slender column with cross section  $Q(x)$  and length  $L_0$ , such  $Q(x)$  must be defined where the buckling load  $F_b$  is maximal,  $F_b = F_{b,max}$ , under the condition that the volume of the optimized column is the same as the volume of the nonoptimized column,  $V_{opt} = V_{const}$ . Prestrain of the martensite phase is the same in both cases. It must be mentioned that  $L_0$  is length of the column before prestrain  $\epsilon_{s0}$  is applied to the column in the martensite phase, and  $L_{s0}$  is the length of the column after prestrain  $\epsilon_{s0}$  is applied.

The aim of our observation is a column with nonconstant cross section, which is prestrained in the martensite temperature region, then simply supported (supports are axially fixed), and heated above  $A_s$ . Due to obstructed temperature dilatation and constrained recovery, there is compressive load in the column, and the column reaches a labile state and eventually buckles. The elastic modulus also changes during the process of constrained recovery above  $A_s$ .

Heating of SMA column must be divided into three regions:

1. First temperature region:  $T_0 \leq T \leq T_c$
2. Second temperature region:  $T_c \leq T \leq T_{c,max}$
3. Third temperature region:  $T_{c,max} \leq T$

where the particular temperature regions will be explained in the following. Constrained recovery is solved using a physical model named *generalized plasticity* (Auricchio and Lubliner, 1996); the model that has been previously used by the authors (Kosel and Videnič, 2007; Videnic et al., 2008). From the static equilibrium of column in axial direction, it is assumed that compressive force is constant over the column's length. Therefore, reverse martensite transformation is located in the greatest area of column, where compressive stress is minimal (Figure 6).

**First Temperature Region:  $T_0 \leq T \leq T_c$**

The variable  $T_0$  is the room temperature and  $T_c$  is the start of reverse martensite transformation, shown in Figures 6 and 7, where it is clear that reverse martensite transformation starts in the column's maximal cross section (cross section 2).

In this temperature region, there is no reverse martensite transformation; however, there is obstructed temperature dilatation, since  $L_s(T)$  is constant during

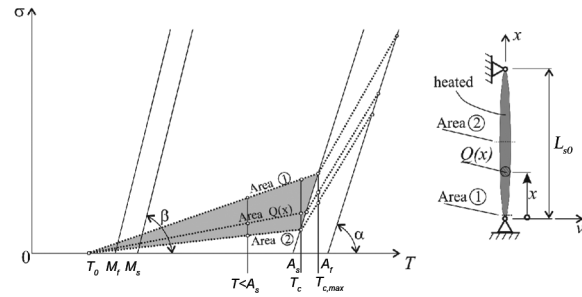


**Figure 6.** Column of nonconstant cross section, stress-temperature relation along the span of SMA column.

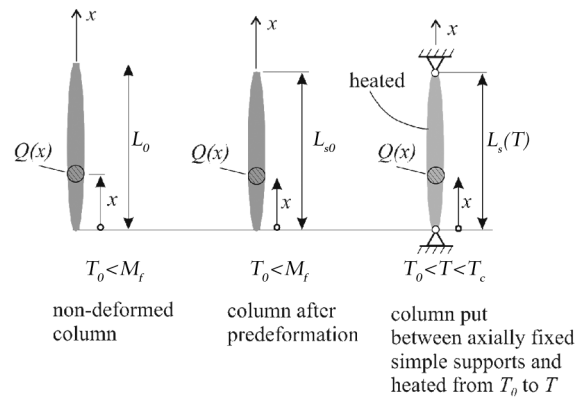


**Figure 7.** Column of nonconstant cross section at different temperatures.

heating, as a result of simple supports fixed in axial direction.

Displacement  $u(T_0 \leq T \leq T_c)$  of the column can be written as

$$u(T) = \epsilon_{s0} \int_0^{L_0} dx + \alpha_s(T - T_0) \int_0^{L_0} dx - \int_0^{L_0} \frac{F dx}{Q(x) E_m} \quad (1)$$

where  $\epsilon_{s0} = (L_{s0} - L_0)/L_0$  is the prestrain of the column in martensite phase ( $T < M_f$ ),  $\alpha_s$  is coefficient of temperature dilatation,  $F$  is compressive force in the column during heating,  $Q(x) = \pi(d(x))^2/4$  is the cross section of the column, while  $E_m$  is elastic modulus of the column. In this temperature region, it is same as elastic modulus of the martensite phase of SMA.

Displacement can be also written as

$$u = L_s(T) - L_0 \quad (2)$$

Equating (1) and (2), expression for  $F$  can be obtained as

$$F = \frac{E_m L_0 (1 + \epsilon_{s0} + \alpha_s(T - T_0))}{\int_0^{L_0} \frac{dx}{Q(x)}} \quad (3)$$

On the other hand,  $F$  can be written as

$$F = \sigma(x, T)Q(x) \tag{4}$$

In order to obtain  $T_c$ , we use the condition for the start of reverse martensite transformation. The model of generalized plasticity (Auricchio and Lubliner, 1996) defines this condition as  $F/Q(x) = C(T_c - A_s)$ , where  $C$  is *stress rate*, experimentally obtained property and presented as  $C = \tan \alpha$  (Figure 6). Equation (4) is checked for this condition and used in Equation (3)

$$C(T_c - A_s)Q(x) = \frac{E_m L_0 (1 + \varepsilon_{s0} + \alpha_s (T_c - T_0))}{\int_0^{L_0} \frac{dx}{Q(x)}} \tag{5}$$

where  $T_c$  is expressed as

$$T_c(x) = \frac{\frac{E_m L_0}{L_0} T_0 - C A_s}{\frac{Q(x) \int_0^{L_0} \frac{dx}{Q(x)}}{\frac{E_m L_0}{L_0} (1 + \varepsilon_{s0} + \alpha_s) - C}} \tag{6}$$

Compressive force in this temperature range is calculated from Equation (3), whereas compressive stress can be calculated using Equations (3) and (4) as

$$\sigma(x, T) = \frac{E_m L_0 (1 + \varepsilon_{s0} + \alpha_s (T - T_0))}{Q(x) \int_0^{L_0} \frac{dx}{Q(x)}} \tag{7}$$

**Second Temperature Region:  $T_c \leq T \leq T_{c,max}$**

$T_{c,max}$  is the minimum temperature where the reverse martensite transformation for the whole column span occurs (Figure 6).

Compressive axial force in the column is caused by two components. The first component is due to obstructed temperature dilatation of the SMA column, and the second is constrained recovery of the SMA column. The total compressive axial force is a function of temperature  $F = N = N(T)$ , and at some temperature, it is constant through the column length,  $N \neq N(x)$ . Due to nonconstant cross section  $Q = Q(x)$ , the compressive stress  $\sigma(x, T) = N(T)/Q(x)$  is a function of the cross section and temperature. The part of the column with lowest compressive stress is the first to achieve the condition for the start of reverse martensite transformation (Figure 8). This part of the column has a length  $2\Delta x$ .

The rest of the column at this temperature remains in martensite phase. The situation for the nondeformed column is presented in Figure 9, and for this situation, we can write the equation for displacement as follows:

$$u_1 + u_2 = L_s(T) - L_0 \tag{8}$$

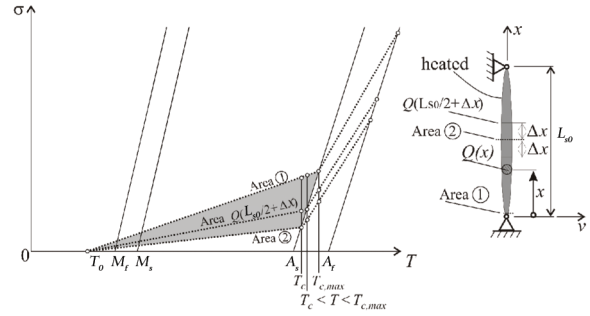


**Figure 8.** Tensile stress versus temperature for various values of span  $x$  of SMA column.

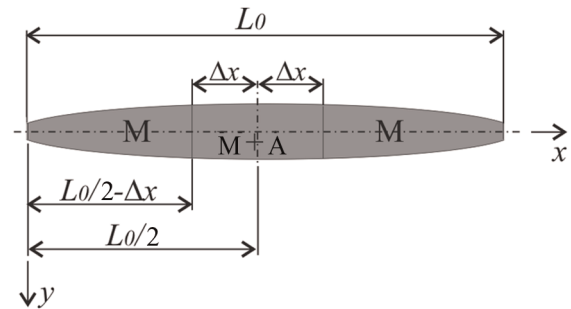


**Figure 9.** Column with nonconstant cross section with exposed region of reverse martensite transformation.

where

$u_1$  is the displacement of region with reverse martensite transformation (M + A)

$u_2$  is the displacement of region without reverse martensite transformation (M)

$$u_1(T) = 2 \left[ \varepsilon_{s0} \int_{\frac{L_0}{2} - \Delta x}^{\frac{L_0}{2}} \xi(x, T) dx + \alpha_s (T - T_0) \int_{\frac{L_0}{2} - \Delta x}^{\frac{L_0}{2}} dx - \int_{\frac{L_0}{2} - \Delta x}^{\frac{L_0}{2}} \frac{F dx}{Q(x)E(x, T)} \right] \tag{9}$$

$$u_2(T) = 2 \left[ \varepsilon_{s0} \int_0^{\frac{L_0}{2} - \Delta x} dx + \alpha_s (T - T_0) \int_0^{\frac{L_0}{2} - \Delta x} dx - \int_0^{\frac{L_0}{2} - \Delta x} \frac{F dx}{Q(x)E_m} \right] \tag{10}$$

In Equations (9) and (10), the  $\xi(x, T)$  is volume fraction of martensite in the SMA, which can be calculated by the equation used in the model of generalized plasticity (Auricchio and Lubliner, 1996):

$$\xi(x, T) = \frac{F(T)}{C(A_f - A_s)Q(x)} + \frac{A_f - T}{A_f - A_s} \tag{11}$$



The elastic modulus for SMA during the phase transformation,  $E(x, T)$ , is calculated by the equation presented by Brinson and Huang (1996):

$$E(x, T) = (E_m - E_a)\xi(x, T) + E_a \quad (12)$$

Equations (9) and (10) can be rearranged and put into Equation (8):

$$\begin{aligned} & L_0(1 + \alpha_s(T - T_0)) \\ & + \varepsilon_{s0} \left[ L_0 - 2\Delta x + \frac{2F}{C(A_f - A_s)} \int_{\frac{L_0}{2} - \Delta x}^{\frac{L_0}{2}} \frac{dx}{Q(x)} + 2 \frac{A_f - T}{A_f - A_s} \Delta x \right] \\ & - \frac{2F}{E_m} \left( \int_0^{\frac{L_0}{2} - \Delta x} \frac{dx}{Q(x)} \right) - 2FC(A_f - A_s) \\ & \int_{\frac{L_0}{2} - \Delta x}^{\frac{L_0}{2}} \frac{dx}{C[E_a(A_f - A_s) - (E_a - E_m)(A_f - T)]Q(x) - (E_a - E_m)F} \\ & = L_{s0} \end{aligned} \quad (13)$$

There are three unknowns in Equation (13):  $\Delta x$ ,  $T$ , and  $F$ . Therefore, we use the condition for the start of reverse martensite transformation (Figure 9):

$$\frac{F(T)}{CQ\left(\frac{L_0}{2} - \Delta x\right)} - C(T - A_s) = 0$$

and express temperature  $T$

$$T = A_s + \frac{F(T)}{CQ\left(\frac{L_0}{2} - \Delta x\right)} \quad (14)$$

Now we can write  $F$  from Equation (13) as

$$\begin{aligned} F(T) = & \frac{-\alpha_s(A_s - T_0)L_0}{\frac{\alpha_s L_0}{CQ\left(\frac{L_0}{2} - \Delta x\right)} + \frac{2\varepsilon_{s0}B_1}{C(A_f - A_s)Q\left(\frac{L_0}{2} - \Delta x\right)} - \frac{2B_2}{E_m} - 2C(A_f - A_s)B_3} \end{aligned} \quad (15)$$

where

$$B_1 = \int_{\frac{L_0}{2} - \Delta x}^{\frac{L_0}{2}} \frac{dx}{Q(x)} \quad (16)$$

$$B_2 = \int_0^{\frac{L_0}{2} - \Delta x} \frac{dx}{Q(x)} \quad (17)$$

$$\begin{aligned} B_3 = & \int_{\frac{L_0}{2} - \Delta x}^{\frac{L_0}{2}} \frac{dx}{C[E_a(A_f - A_s) - (E_a - E_m)(A_f - T)]Q(x) - (E_a - E_m)F} \end{aligned} \quad (18)$$

### Third Temperature Region: $T \geq T_{c,max}$

When  $T \geq T_{c,max}$ , the reverse martensitic transformation takes place in all parts of the SMA column. The condition for this region is therefore  $\sigma_s(\Delta x = L_0/2, T_{c,max}) \geq C(T_{c,max} - A_s)$ . In this temperature region, equations from the second temperature region are used, where  $\Delta x = L_0/2$ . Temperature  $T$  in this region is taken as variable, and we use Equation (12) to express  $F$  as

$$F = \frac{L_{s0} + \varepsilon_{s0}L_0 \frac{A_f - T}{A_f - A_s} - L_0(1 + \alpha_s(T - T_0))}{\frac{2B_1\varepsilon_{s0}}{C(A_f - A_s)} + 2CB_3(A_f - A_s)} \quad (19)$$

where it is considered  $B_2(L_0/2) = 0$ ,

## Calculation of Buckling Force and Temperature for the Optimized SMA Column

### Obtaining the Function of Cross Section $Q(x)$ for SMA Column

In the previous section, equations for obtaining the compressive force as a function of temperature during constrained recovery were obtained for an arbitrary function of column cross section  $Q(x)$  and for any form of cross section. Due to some limitations in experiments, we chose a particular shape of the optimized column (Figure 10). Three distinct regions of the optimized column can be noticed: two regions  $L_1/2$  with diameter  $d_1$ , and region  $L_2$  with diameter  $d_2$ , where  $L_1 + L_2 = L_0$ .

Let us first calculate  $d_2$ , such that the volume of the optimized column equals the volume of nonoptimized column of same length,  $V_{opt} = V_{const}$ , and we can express  $d_2$

$$d_2 = \sqrt{\frac{D_{const}^2(L_1 + L_2) - d_1^2L_1}{L_2}} \quad (20)$$

where  $D_{const}$  is the diameter of the nonoptimized column.

### Calculation of Function $F(T)$ and $E(x, T)$

In order to calculate the compressive force in the member during heating, we must obtain integrals in Equations (16)–(19). We must obtain two sets of solutions, which depend on the length  $\Delta x$ .

For each region of the column, the cross section is written as

$$Q_1 = \frac{\pi d_1^2}{4} \quad \text{and} \quad Q_2 = \frac{\pi d_2^2}{4} \quad (21)$$



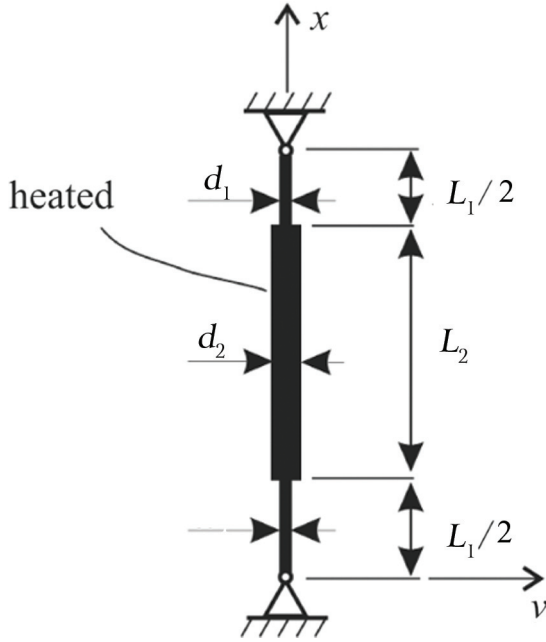


**Figure 10.** Simply supported column with nonconstant circular cross section.

Calculation of  $B_1$  :

1. For  $\Delta x < L_2/2$  :

$$B_1 = \frac{\Delta x}{Q_2} \quad (22)$$

2. For  $\Delta x > L_2/2$  :

$$B_1 = \frac{L_2 - L_0}{4Q_2} + \frac{\Delta x - \frac{L_2}{2}}{Q_1} \quad (23)$$

Calculation of  $B_2$  :

1. For  $\Delta x < L_2/2$  :

$$B_2 = \frac{L_1}{2Q_1} + \frac{L_0 - L_1 + L_2}{4Q_2} \quad (24)$$

2. For  $\Delta x > L_2/2$  :

$$I_2 = \frac{1}{4} \frac{L_0 - L_2}{Q_1} \quad (25)$$

Calculation of  $B_3$ :

1. For  $\Delta x < L_2/2$  :

$$B_3 = \frac{\Delta x}{C[E_a(A_f - A_s) - (E_a - E_m)(A_f - T)]Q_2 - (E_a - E_m)F} \quad (26)$$

2. For  $\Delta x > \frac{L_2}{2}$  :

$$B_3 = \frac{L_2}{2C[E_a(A_f - A_s) - (E_a - E_m)(A_f - T)]Q_2 - (E_a - E_m)F} + \frac{\Delta x - \frac{L_2}{2}}{C[E_a(A_f - A_s) - (E_a - E_m)(A_f - T)]Q_1 - (E_a - E_m)F} \quad (27)$$

### Obtaining Critical Buckling Force and Critical Buckling Temperature

From the results of additional compressive loading, we have already shown that it is correct to deal with buckling of the column by considering that for SMA at buckling temperature  $T_b$ , the additional compressive stress is linear function of compressive strain (Figure 4). Therefore, we can use the known method for obtaining the buckling force of the elastic column with small deflection theory.

For simply supported column with three different regions (Figure 10), the buckling force  $F_b$  is calculated from the transcendent equation, presented by Timoshenko (1961):

$$\sqrt{\frac{E_{d2}I_{d2}}{E_{d1}I_{d1}}} = \tan\left(\frac{\omega_2 L_2}{2}\right) \tan\left(\frac{\omega_2 L_1}{2} \sqrt{\frac{E_{d2}I_{d2}}{E_{d1}I_{d1}}}\right) \quad (28)$$

where

$$\omega_2^2 = \frac{F_b}{E_{d2}I_{d2}} \quad (29)$$

where  $E_{d1}$  and  $I_{d1}$  are elastic modulus and minimum second moment of area for cross section in region with  $d_1$ ;  $E_{d2}$  and  $I_{d2}$  are elastic modulus and minimum second moment of area in region with  $d_2$ .

The procedure for obtaining the buckling force and buckling temperature is as follows: we have to solve the system of three nonlinear equations with three unknowns (buckling force  $F_b$ , buckling temperature  $T_b$ , and elastic modulus  $E$  during buckling). First equation in this system is selected among Equations (3), (14), or (18). Selection is made with respect to the temperature region in which the column is presented at the observed temperature. Second in the system is Equation (12), the equation for obtaining elastic modulus  $E(x, T)$ . Third equation in the system is Equation (27). In this system of equations, it is assumed that  $F(T_b) = F_b(T_b)$ , namely, the compressive force  $F$  in the column at buckling temperature  $T_b$  equals buckling force  $F_b$  at buckling temperature  $T_b$ .

## Experimental Verification of Calculated Buckling Temperatures

### Introduction

Verification of the calculated buckling forces and temperatures for various shapes of columns was performed

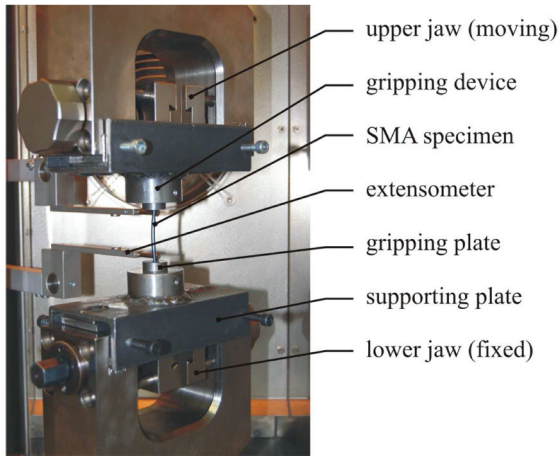


Figure 11. Buckled specimen in the testing machine.

by experiments described in the following. A special gripping plate, which provided a simple support, was made for the experiment—a shallow hole was drilled into the plate to ensure the hinge between the specimen and plate. The specimen had both end surfaces ground in spherical shape. Oil was put in the hole to reduce friction between the specimen and plate.

The testing procedure consists of three main stages: The first and second stages are identical to the first two stages presented in section ‘Test Procedure’. In the third stage, the specimen was put between the aforementioned gripping plate, as shown in Figure 11. The software kept the distance between the extensometers constant during the test. Extensometers were put on the specimen body between the clamping jaws. Air temperature in the temperature chamber started to rise at a rate of 1°C/min. The temperature was rising until buckling of the specimen occurred, as shown in Figure 11, and then the temperature was left to rise by a few degrees Celsius more. The rise of the temperature was conducted with one purpose alone—to evidence the buckling temperature from the sudden change in diagram ‘temperature–tensile force’; however, buckling of the specimen was also observed by naked eye.

The geometry of the optimized column is presented in Figure 10, whereas the nonoptimized column is of the same length and constant diameter  $D_{\text{const}}$ . Let us explain that searching of the optimal column among the optimized samples was specific, since not all samples had the same volume. Samples were compared in pairs of one optimized column and one nonoptimized column (both columns have the same volume,  $V_{\text{opt}} = V_{\text{const}}$ ), as shown in Table 1. The reason for not making all the samples with the same volume is due to difficulty of experiments and due to limited diameter, which could not exceed 3 mm. Therefore, we cannot compare the absolute value of the buckling force for all samples. On the other hand, we can

Table 1. Diameter of nonoptimized column for different lengths  $L_1/2$ .

	$L_1/2$ (mm)	$D_{\text{const}}$ (mm)	Volume (mm <sup>3</sup> )
First pair	4	2.907	265.5
Second pair	6	2.859	256.8
Third pair	10	2.77	241.1

For every column the total length is the same,  $L_{s0} = 40$  mm.

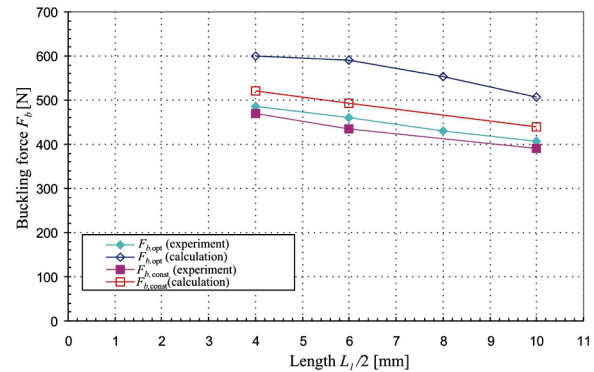


Figure 12. Calculated and measured buckling force  $F_b$  as function of  $L_1/2$  for optimized and nonoptimized column.

observe the effect of length  $L_1/2$  on the buckling force and temperature for each pair, and by doing this, we can still obtain optimal length  $L_1/2$ , namely the shape of optimized column. Six groups of experiments were designed, each group consisted of three experiments for one sample. In one of the groups, only two experiments were designed. Additional sample is the one with  $L_1/2 = 8$  mm, and for this sample, three buckling experiments were performed.

## Results

Physical properties were obtained in experiments, their values are as follows:  $E_m = 24$  GPa,  $E_a = 43$  GPa,  $A_s = 57^\circ\text{C}$ ,  $A_f = 67^\circ\text{C}$ ,  $C = 5.6$  MPa/°C,  $\varepsilon_{s0} = 2\%$  (compressive prestrain),  $\alpha_s = 4.4 \times 10^{-5}$  1/K,  $L_{s0} = 40$  mm,  $d_1 = 2.5$  mm, and  $d_2 = 3$  mm.

Figures 12 and 13 shows the calculated and averaged experimental results. From Figure 14, it is clear that maximum ratio between the buckling force of the optimized and nonoptimized column appears at  $L_1/2 = 6$  mm, and this length is the same for the calculated and experimental results. The experimentally obtained buckling force for the optimal column is only 5.7% higher than that of the nonoptimized column, while from calculated results it is expected as 19%. Figure 15 shows that the ratio between the buckling temperature of the optimized and nonoptimized column is also maximal at  $L_1/2 = 6$  mm, but in this case

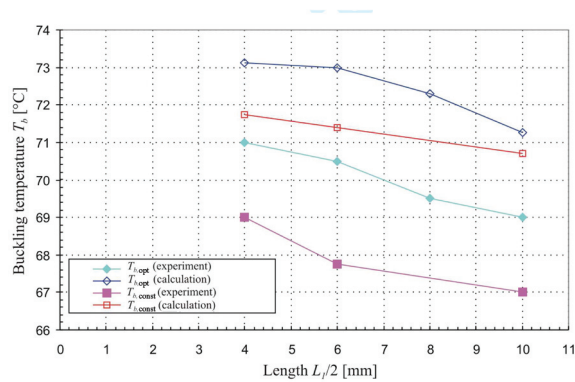


**Figure 13.** Calculated and measured buckling temperature  $T_b$  as function of  $L_1/2$  for optimized and nonoptimized column.

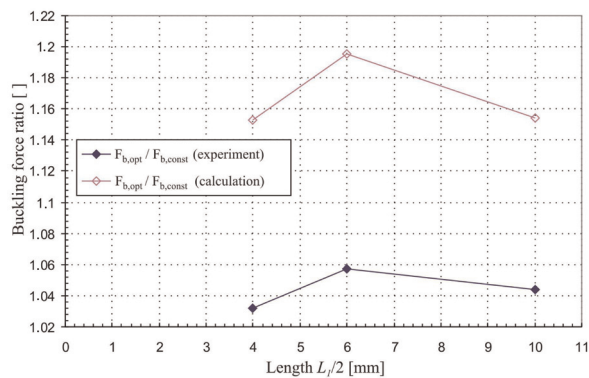


**Figure 14.** Ratio between buckling force  $F_b$  of optimized and nonoptimized column as function of  $L_1/2$  for experimental and calculated results, respectively.

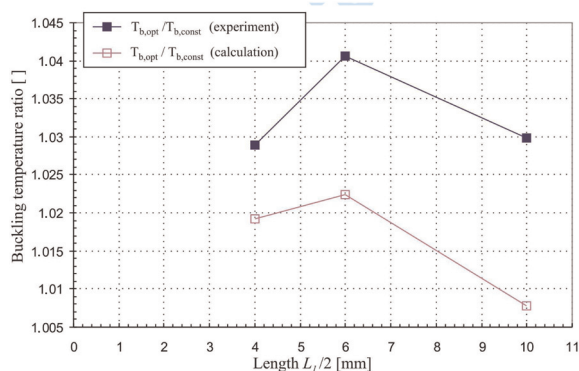


**Figure 15.** Ratio between buckling temperature of optimized and nonoptimized column as function of  $L_1/2$  for experimental and calculated results, respectively.

we observe a small increase (4% and 1.8%) in the buckling temperature at experiments and calculation, respectively.

In general, experimental measures and numerical results of buckling temperature show good agreement, which was the main goal of this research. This is because, it is most important to predict the precise temperature of buckling for the potential use of the SMA column in the thermostwitch. Moreover, it was proven that in circumstances where constant temperature of buckling is requested even if the shape of the column is not precisely constant over the length, the phenomenon of buckling of SMA column could be used.

However, there is discrepancy between experimental measures and numerical results of buckling force for optimized column, and we see two possible reasons for this. First, prestrain over the length of the SMA column is not precisely known; however, in the model, it is assumed to be constant. Obviously, it is impossible to experimentally achieve that prestrain is constant for the whole SMA column, since the SMA column had nonconstant area. More precise numerical results could be expected if this fact was assumed in the model, but in this case, new sets of experiments would be needed to obtain values of elastic modulus, which is also a function of the prestrain. Second, there were few difficulties with keeping the optimized column in ideally straight shape during the prestraining; therefore, there is a chance that initial nonzero curvature could be present in the SMA column, but it was not assumed in the model.

## Conclusion

This article reports on research work in the field of compression properties of SMAs during constrained recovery. Compressive force in an SMA column during constrained recovery is calculated as function of temperature for an arbitrary function of cross section along the span of the SMA column with arbitrary shape of column's cross section. The elastic modulus as function of temperature is calculated for the whole span of the column with nonconstant cross section. Optimization of geometry is made for the column with a circular cross section and by choosing particular shape of column (Figure 10), where our goal was to obtain optimal length  $L_1/2$ . Considering experimental results, the equation for elastic buckling for the column with nonconstant cross section was proposed and used to calculate the buckling force and temperature. The calculated buckling force and temperature show good agreement with buckling experiments; however, possible modifications of the model are a matter of the work in future. The experimental buckling force of the optimal column is not much higher than the buckling force of the constant column; therefore, searching for an even more optimal shape of the column is a matter of future work.

## References

- Auricchio F and Lubliner J (1996) A generalized plasticity and shape-memory alloys. *International Journal of Solids and Structures* 33: 991–1003.
- Bažant Z and Cedolin L (1991) *Stability of Structures*. New York: Oxford University Press.
- Brinson LC (1993) One-dimensional constitutive behavior of shape memory alloys: Thermomechanic derivation with non-constant material functions and redefined martensite internal variable. *Journal of Intelligent Material Systems and Structures* 4: 229–242.
- Brinson LC and Huang MS (1996) Simplifications and comparisons of shape memory alloy constitutive models. *Journal of Intelligent Material Systems and Structures* 7: 108–114.
- Duerig TW, Melton KN, Stöckel D, and Wayman CM (1990) *Engineering Aspects of Shape Memory Alloys*. London: Butterworth–Heinemann.
- Duerig T, Pelton A and Stöckel D (1999) An overview of nitinol medical applications. *Materials Science and Engineering: A* 273–275: 149–160.
- Kato H, Inagaki N and Sasaki K (2004) A one-dimensional modelling of constrained shape memory effect. *Acta Materialia* 52: 3375–3382.
- Kosel F and Videnič T (2007) Generalized plasticity and uniaxial constrained recovery in shape memory alloys. *Mechanics of Advanced Materials and Structures* 14(1): 3–12.
- Lee HY and Jung JL (1999) A simulation study on the thermal buckling behavior of laminated composite shells with embedded shape memory alloy (SMA) wires. *Composite Structures* 47: 463–469.
- Movchan AA and Sil'chenko LG (2003) Buckling of a rod undergoing direct or reverse martensite transformation under compressive stresses. *Journal of Applied Mechanics and Technical Physics* 44(3): 442–449.
- Rahman MA, Qiu J and Tani J (2001) Buckling and post-buckling characteristics of the superelastic SMA columns. *International Journal of Solids and Structures* 38: 9253–9265.
- Rahman MA, Qiu J and Tani J (2005) Buckling and post-buckling characteristics of the superelastic SMA columns—Numerical simulation. *Journal of Intelligent Material Systems and Structures* 16: 691–702.
- Shanley FR (1957) *Strength of Materials*. New York: McGraw-Hill.
- Šittner P, Vokoun D, Dayananda GN, Stalmans R (2000) Recovery stress generation in shape memory  $\text{Ti}_{50}\text{Ni}_{45}\text{Cu}_5$  thin wires. *Metal Science and Engineering A* 286: 298–311.
- Stalmans R, Van Humbeeck J and Delaey L (1997) Generation of recovery stresses: Thermodynamic modelling and experimental verification. *Journal de Physique IV C5*: 47–52.
- Timoshenko SP (1961) *Theory of Elastic Stability*. New York: McGraw-Hill.
- Videnič T, Franc K, Viktor S and Miha B (2008) Biaxial constrained recovery in shape memory alloy rings. *Journal of Intelligent Materials System and Structures* 19(8): 861–874.